Generalized Non-rigid Point Set Registration with Hybrid Mixture Models Considering Anisotropic Positional Uncertainties

Chapter · October 2019

DOI: 10.1007/978-3-030-32254-0_61

3 authors, including:

Zhe Min
The Chinese University of Hong Kong
21 PUBLICATIONS **71** CITATIONS

SEE PROFILE

Generalized Non-rigid Point Set Registration with Hybrid Mixture Models Considering Anisotropic Positional Uncertainties

Zhe Min[1(✉)], Li Liu[1], and Max Q.-H. Meng[1,2]

[1] Robotics, Perception, and Artificial Intelligence Lab,
The Chinese University of Hong Kong, Shatin, NT, Hong Kong, China
{zmin,max}@ee.cuhk.edu.hk
[2] Shenzhen Research Institute,
The Chinese University of Hong Kong, Shenzhen, China
liliu@cuhk.edu.hk

Abstract. Image-to-patient or pre-operative to intra-operative registration is an essential problem in computer-assisted surgery (CAS). Non-rigid or deformable registration is still a challenging problem with partial overlapping between point sets due to limited camera view, missing data due to tumor resection and the surface reconstruction error intra-operatively. In this paper, we propose and validate a normal-vector assisted non-rigid registration framework for accurately registering soft tissues in CAS. Two stages including rigid and non-rigid registrations are involved in the framework. In the stage of the rigid registration that does the initial alignment, the normal vectors extracted from the point sets are used while the position uncertainty is assumed to be anisotropic. With the normal vectors incorporated, the algorithm can better recover the point correspondences and is more robust to intra-operative partial data which is often the case in a typical laparoscopic surgery. In the stage of the non-rigid registration, the anisotropic coherent point drift (CPD) method is formulated, where the isotropic error assumption is generalized to anisotropic cases. Extensive experiments on the human liver data demonstrate our proposed algorithm's several great advantages over the existing state-of-the-art ones. First, the rigid transformation matrix is recovered more accurately. Second, the proposed registration framework is much more robust to partial scan. Besides, the anisotropic CPD outperforms the original CPD significantly in terms of robustness to noise.

1 Introduction

Registration is an essential problem in both medical imaging (MI) and computer assisted surgery (CAS) or image-guided surgery (IGS). Registration problems

Electronic supplementary material The online version of this chapter (https://doi.org/10.1007/978-3-030-32254-0_61) contains supplementary material, which is available to authorized users.

D. Shen et al. (Eds.): MICCAI 2019, LNCS 11768, pp. 547–555, 2019.
https://doi.org/10.1007/978-3-030-32254-0_61

can be coarsely divided into rigid registrations and non-rigid registrations. In a rigid registration, the transformation is rigid, which typically includes a rotation matrix, a translation vector. In a non-rigid registration, the transformation between PSs is usually unknown and nonlinear. Compared with the rigid one, the non-rigid registration is a much more challenging problem [4,14,15].

In IGS, the pre-operative CT or MRI model has to be accurately registered with the intra-operative scan data (or so-called image-to-patient registration). This vital task especially the non-rigid registration is still challenging because of the initial pose between the two point sets (PSs), partial overlapping because of the partial visible surface during surgery, and the noisy sensor data (both pre-operatively and intra-operatively). More specifically, the camera attached to the surgical instrument only has access to a restricted region of the abdomen in a typical laparoscopic surgery [14] and the surface data from the stereo reconstruction intra-operatively is very noisy [14]. The rigid PS registration is utilized to recover the initial gross misalignment between the pre-operative and intra-operative spaces [13,14]. In terms of non-rigid registration, brain shift usually exists in the neuro-surgical procedures such as tumor resection [1]. In image-guided liver surgery (IGLS), the deformation of the liver intra-operatively comes from organ shape changes, respiration, liver mobilization, and resection [3].

Recently, Ravikumar et al. generalized the coherent point drift (CPD) method to high-dimensional points for the group-wise registration problem [12,13]. Bayer et al. adopts and reformulates the method in [13] to compensate the brain shift in a neuro-surgical procedure such as tumor resection [1]. In both stages of rigid registration and non-rigid registrations in [1,12,13], the isotropic localization error assumption is shared. However, this ideal and simple assumption actually does not fit the real scenarios in surgical navigation. For example, in a stereo camera system (such as an endoscopy or laparoscopy), the standard deviation of the point localization error in the viewing direction is three or five times than those in the other two directions [5,10]. Very recently, Min et al. considered the anisotropic positional uncertainty in the pair-wise rigid registration [10], and later for the multiple point set registration problems [6].

In this paper, we present a novel non-rigid registration framework based on the use of normal vectors and the anisotropic assumption of positional uncertainty. On one hand, the normal vectors are used to enhance the registration performance, which brings several benefits. First, the posterior probabilities representing the point correspondences can be computed more accurately. Second, the rotation matrix that aligns two point sets can be recovered more accurately. On the other hand, the anisotropic uncertainty is considered in both rigid and non-rigid registrations. The main contributions of our work are: (1) the normal-vector assisted rigid registration algorithm considering the anisotropic positional uncertainty is formally introduced in the proposed non-rigid registration framework; (2) to the best of our knowledge, the anisotropic non-rigid CPD is formulated and validated for the first time; (3) extensive simulated experiments on the human liver data sets are conducted to validate the proposed algorithms.

2 Methods

One surface represented by point sets (PSs) $\mathbf{X} = [\mathbf{x}_1, ...\mathbf{x}_n..., \mathbf{x}_N] \in \mathbb{R}^{3\times N}$ that has been deformed is registered with the initial one $\mathbf{Y} = [\mathbf{y}_1, ...\mathbf{y}_m..., \mathbf{y}_M] \in \mathbb{R}^{3\times M}$. The transformation between $\mathbf{X}$ and $\mathbf{Y}$ could possibly include a rigid transformation. Our proposed registration framework is overall divided into two stages: rigid and non-rigid registrations. In both stages, the registrations are formulated as maximum likelihood (ML) problems with the hidden variables being the point correspondences, and are solved under the expectation maximization (EM) framework. At the beginning of the first stage, the unit normal vector sets $\widehat{\mathbf{X}} = [\widehat{\mathbf{x}}_1, ...\widehat{\mathbf{x}}_n..., \widehat{\mathbf{x}}_N]$ and $\widehat{\mathbf{Y}} = [\widehat{\mathbf{y}}_1, ...\widehat{\mathbf{y}}_m..., \widehat{\mathbf{y}}_M]$ are extracted from $\mathbf{X}$ and $\mathbf{Y}$, where $\widehat{\mathbf{x}}_n \in \mathcal{S}^2$ and $\widehat{\mathbf{y}}_m \in \mathcal{S}^2$. Two generalized PSs are then constructed as $\mathbf{D}_x = [\mathbf{d}_1^x, ...\mathbf{d}_n^x..., \mathbf{d}_N^x]$ and $\mathbf{D}_y = [\mathbf{d}_1^y, ...\mathbf{d}_n^y..., \mathbf{d}_N^y]$, where $\mathbf{d}_n^x = (\mathbf{x}_n, \widehat{\mathbf{x}}_n)^\mathsf{T}$ and $\mathbf{d}_m^y = (\mathbf{y}_m, \widehat{\mathbf{y}}_m)^\mathsf{T}$ are both six-dimensional vectors. After the first stage, the rigid transformation including the rotation matrix $\mathbf{R} \in SO(3)$ and translation vector $\mathbf{t} \in \mathbb{R}^3$, the updated posterior probabilities and covariance matrix $\mathbf{\Sigma} \in \mathbb{S}^3$ are acquired and used in the following non-rigid stage. The model parameters in the stages of rigid and non-rigid registrations are defined as $\mathbf{\Theta} = \{\mathbf{R}, \mathbf{t}, \mathbf{\Sigma}\}$ and $\mathbf{\Theta}_p = \{v, \mathbf{\Sigma}\}$ respectively. Those parameters will be illustrated in the following.

2.1 Generalized Rigid Point Set Registration Considering Anisotropic Positional Uncertainty (HMM (Anisotropic))

Multi-Variate Gaussian and Von-Mises Fisher (VMF) distributions are used to model the positional and normal error vectors respectively [10]. By assuming that the positional and normal vectors are independent, the probability density function (PDF) of a generalized data point $\mathbf{d}_n^x$ given the current correspondence $z_n = m$ is defined in (1), where $\mathbf{z}_{mn} = \mathbf{x}_n - \mathbf{R}\mathbf{y}_m - \mathbf{t} \in \mathbb{R}^3$, $|\bullet|$ denotes the determinant of a matrix, the concentration parameter κ controls how $\widehat{\mathbf{x}}_n$ distribute about the central one $\mathbf{R}\widehat{\mathbf{y}}_m$. More specifically, the larger the value of κ is the more concentrated the sampled normal vectors are. The hybrid mixture models (HMMs) defined as $p(\mathbf{d}_n^x|\mathbf{D}_y, \mathbf{\Theta}) = w\frac{1}{N} + (1-w)\sum_{m=1}^{M}\frac{1}{M}p(\mathbf{d}_n^x|z_n = m)$ are the sum of an additional uniform distribution to account for noise or outliers and the PDF in (1). The weighting factor $w \in \mathbb{R}$ denotes the weight of the uniform distribution, and the prior probability of all the mixture components is $\frac{1}{M}$. By assuming that the data points in $\mathbf{D}_x$ are independent, the data likelihood defined as $\mathcal{L}(\mathbf{\Theta}) = \prod_{i=1}^{n} p(\mathbf{d}_n^x|\mathbf{D}_y, \mathbf{\Theta})$ is the product of the data points' PDFs. Instead of maximizing $L(\mathbf{\Theta})$, to estimate $\mathbf{\Theta}$, the expected negative log likelihood function (llh) is often minimized, which is $Q(\mathbf{\Theta})$ in (2) by ignoring the constants independent of $\mathbf{\Theta}$. In (2), $N_\mathbf{P} = \sum_{n=1}^{N}\sum_{m=1}^{M} p_{mn}$, where $p_{mn} \in \mathbb{R}$ is the posterior probability and is updated using the Bayes' rule as $p_{mn} = \frac{\frac{1}{M}p(\mathbf{d}_n^x|z_n=m)}{p(\mathbf{d}_n^x|\mathbf{D}_y,\mathbf{\Theta})}$ (E-step). The updated $\mathbf{\Sigma}$ is computed by solving $\frac{\partial Q(\mathbf{\Theta})}{\partial \mathbf{\Sigma}} = \mathbf{0}$ in (2) (M-step). The updated κ is computed by solving $\frac{\partial Q(\mathbf{\Theta})}{\partial \kappa} = 0$ $(-\frac{1}{\kappa} + \frac{e^\kappa + e^{-\kappa}}{e^\kappa - e^{-\kappa}} = \frac{1}{N_\mathbf{P}}\sum_{m=1}^{M}\sum_{n=1}^{N} p_{mn}(\mathbf{R}\widehat{\mathbf{y}}_m)^\mathsf{T}\widehat{\mathbf{x}}_n)$, which is solved using the fixed

point approach (M-step). E and M steps will iterate until convergence. In the end, the transformed model PS is $\mathbf{T}(\mathbf{Y}) = [\mathbf{R}\mathbf{y}_1 + \mathbf{t}, ...\mathbf{R}\mathbf{y}_m + \mathbf{t}..., \mathbf{R}\mathbf{y}_M + \mathbf{t}] \in \mathbb{R}^{3\times M}$.

$$p(\mathbf{d}_n^x | z_n = m, \boldsymbol{\Theta}) = \underbrace{\frac{1}{(2\pi)^{\frac{3}{2}}|\boldsymbol{\Sigma}|^{\frac{1}{2}}} e^{-\frac{1}{2}(\mathbf{z}_{mn}))^{\mathsf{T}}\boldsymbol{\Sigma}^{-1}(\mathbf{z}_{mn})}}_{\text{Position Vectors}} \cdot \underbrace{\frac{\kappa}{2\pi(e^{\kappa} - e^{-\kappa})} e^{\kappa(\mathbf{R}\widehat{\mathbf{y}}_m)^{\mathsf{T}}\widehat{\mathbf{x}}_n}}_{\text{Normal Vectors}}, \tag{1}$$

$$\begin{aligned} Q(\boldsymbol{\Theta}) = &\sum_{n=1}^{N}\sum_{m=1}^{M} p_{mn}\Big(\frac{1}{2}\big(\mathbf{x}_n - \mathbf{R}\mathbf{y}_m - \mathbf{t}\big)^{\mathsf{T}}\boldsymbol{\Sigma}^{-1}\big(\mathbf{x}_n - \mathbf{R}\mathbf{y}_m - \mathbf{t}\big) - \kappa(\mathbf{R}\widehat{\mathbf{y}}_m)^{\mathsf{T}}\widehat{\mathbf{x}}_n\Big) \\ &+ \frac{1}{2}N_{\mathbf{P}}\log|\boldsymbol{\Sigma}| + N_{\mathbf{P}}\log\big(e^{\kappa} - e^{-\kappa}\big) - N_{\mathbf{P}}\log\kappa. \end{aligned} \tag{2}$$

2.2 Non-rigid Point Set Registration Considering Anisotropic Positional Uncertainty (Anisotropic CPD)

The rigidly aligned model $\mathbf{T}(\mathbf{Y})$ is used as an input in this stage, but is still denoted as $\mathbf{Y}$ for simplicity. The non-rigid transformation is assumed to be the initial position plus some displacement function v (i.e the warped model PS $\mathbf{T}(\mathbf{Y}) = \mathbf{Y} + v(\mathbf{Y}) \in \mathbb{R}^{3\times M}$). The non-rigid transformation is further regularized using Tikhonov regularization, and expressed in the Reproducing Kernel Hilbert Space(RKHS)[11]. Considering the anisotropic positional uncertainty, the PDF of one data point $\mathbf{x}_n$ given the current correspondence (i.e. $z_n = m$) is defined as (3). Similar to Sect. 2.1, the mixture model is expressed as $p(\mathbf{x}_n|\mathbf{Y}, \boldsymbol{\Theta}_p) = w\frac{1}{N} + (1-w)\sum_{m=1}^{M}\frac{1}{M}p(\mathbf{x}_n|z_n = m)$. Assuming that points in $\mathbf{X}$ are independent, the data likelihood $\mathcal{L}(\boldsymbol{\Theta}_p)$ is the product of the PDFs associated with $\mathbf{x}_n$: $\mathcal{L}(\boldsymbol{\Theta}_p) = \prod_{i=1}^{n} p(\mathbf{x}_n|\mathbf{Y}, \boldsymbol{\Theta}_p)$. The expected negative log-likelihood $Q(\boldsymbol{\Theta}_p)$ defined in (4) is minimized to seek $\boldsymbol{\Theta}_p$. In (4), $\mathbf{z}_{mn}^{\text{deform}}\big(\mathbf{x}_n - \mathbf{y}_m - v(\mathbf{y}_m)\big) \in \mathbb{R}^3$, $\lambda \in \mathbb{R}$ denotes the weight of the regularization term, and the operator P "extracted" the high frequency content part of v. As proved in [11], the function v that minimizes $Q(\boldsymbol{\Theta}_p)$ is a linear combination of radial basis functions (RBFs). To significantly facilitate the computation, the matrix form of $Q(\mathbf{W})$ is presented in (5), where $\mathrm{tr}(\bullet)$ denotes the trace of a matrix and $\mathbf{P} \in \mathbb{R}^{M\times N}$ stores the posteriors with $p_{mn} = \frac{\frac{1}{M}p(\mathbf{x}_n|z_n=m,\boldsymbol{\Theta}_p)}{p(\mathbf{x}_n|\mathbf{Y},\boldsymbol{\Theta}_p)}$ (E-step). In (5), $\mathbf{W} \in \mathbb{R}^{M\times 3}$ is the matrix of coefficients associated with RBFs while $\mathbf{G} \in \mathbb{S}^{M\times M}$ is a kernel matrix with elements $g_{ij} = G(\mathbf{y}_i, \mathbf{y}_j) = e^{-\frac{1}{2}||\frac{\mathbf{y}_i - \mathbf{y}_j}{\beta}||^2}$, where $\beta \in \mathbb{R}$ is the kernel bandwidth controlling PSs' local structure. By computing $\frac{\partial Q(\mathbf{W})}{\partial \mathbf{W}} = \mathbf{0}$ in (5) and with some matrix manipulations, we can get $\underbrace{\mathrm{diag}(\mathbf{P1})\mathbf{G}}_{\mathbf{A}}\underbrace{\mathbf{W}}_{\mathbf{X}} + \underbrace{\mathbf{W}}_{\mathbf{X}}\underbrace{\lambda\boldsymbol{\Sigma}}_{\mathbf{B}} = \underbrace{\mathbf{P}\mathbf{X}^{\mathsf{T}} - \mathrm{diag}(\mathbf{P1})\mathbf{Y}^{\mathsf{T}}}_{\mathbf{C}}$ about $\mathbf{W}$, which is solved by solving $\mathbf{AX} + \mathbf{XB} = \mathbf{C}$ in MATLAB (M-step). E and M steps will iterate until convergence. Finally we get $\mathbf{T}(\mathbf{Y}) = \mathbf{Y} + \mathbf{W}^{\mathsf{T}}\mathbf{G}^{\mathsf{T}}$.

$$p(\mathbf{x}_n|z_n = m, \boldsymbol{\Theta}_p) = \frac{1}{(2\pi)^{\frac{3}{2}}|\boldsymbol{\Sigma}|^{\frac{1}{2}}} e^{-\frac{1}{2}\left(\mathbf{x}_n - \mathbf{y}_m - v(\mathbf{y}_m)\right)^{\mathsf{T}}\boldsymbol{\Sigma}^{-1}\left(\mathbf{x}_n - \mathbf{y}_m - v(\mathbf{y}_m)\right)}, \tag{3}$$

$$Q(\boldsymbol{\Theta}_p) = \frac{1}{2}\sum_{n=1}^{N}\sum_{m=1}^{M} p_{mn}\left(\mathbf{z}_{mn}^{\text{deform}}\right)^{\mathsf{T}}\boldsymbol{\Sigma}^{-1}\mathbf{z}_{mn}^{\text{deform}} + \frac{1}{2}N_{\mathbf{P}}\log|\boldsymbol{\Sigma}| + \frac{\lambda}{2}||Pv||^2, \quad (4)$$

$$\begin{aligned} Q(\mathbf{W}) = &-\text{tr}\left(\mathbf{W}^{\mathsf{T}}\mathbf{G}^{\mathsf{T}}\mathbf{P}\mathbf{X}^{\mathsf{T}}\boldsymbol{\Sigma}^{-1}\right) + \text{tr}\left(\mathbf{W}^{\mathsf{T}}\mathbf{G}^{\mathsf{T}}\text{diag}(\mathbf{P1})\mathbf{Y}^{\mathsf{T}}\boldsymbol{\Sigma}^{-1}\right) \\ &+ \text{tr}\left(\mathbf{W}^{\mathsf{T}}\mathbf{G}^{\mathsf{T}}\text{diag}(\mathbf{P1})\mathbf{G}\mathbf{W}\boldsymbol{\Sigma}^{-1}\right) + \frac{\lambda}{2}\text{tr}(\mathbf{W}^{\mathsf{T}}\mathbf{G}\mathbf{W}). \end{aligned} \quad (5)$$

3 Experiments and Results

In the following series of studies, in silico liver data set in OpenCAS[1] is used [16] which contains three liver models that have been deformed by means of a non-linear biomechanical model. For each model, we note that the deformed surface points $\mathbf{X}$ (partial or full) represents the intra-operative data PS while the initial volume points $\mathbf{Y}$ (full) represents the pre-operative model PS. The normal vectors $\widehat{\mathbf{X}}$ and $\widehat{\mathbf{Y}}$ associated with $\mathbf{X}$ and $\mathbf{Y}$ are computed in MeshLab [2] with the number of neighbouring points being 10 (the default value), and afterwards $\mathbf{D}_x$ and $\mathbf{D}_y$ can be acquired afterwards. Note that the directions of the normal vectors are automatically pointing outwards the surfaces using MeshLab.

Rigid Registration Performance. In this section, $\mathbf{Y}$ (or $\mathbf{D}_y$) is rotated using a random rotation matrix $\mathbf{R}^g$ (that corresponds to an angle $\theta = 20°$). For computing efficiency, both $\mathbf{D}_x$ and rotated $\mathbf{Y}$ (or $\mathbf{D}_y$) are downsampled to own $N_{test} = 1000$ points since we have found that down sampling the PSs will not worsen the performance significantly using all registration methods. The inputs to CPD [11] are $\mathbf{X}$ and rotated $\mathbf{Y}$ while the inputs to HMM(isotropic) [7,9] and HMM(anisotropic) introduced in Sect. 2.1 are $\mathbf{D}_x$ and rotated $\mathbf{D}_y$. The rotational error values in degree are computed[2]. The above process is repeated for $N_{\text{repeat}} = 1000$ times, and afterwards the mean and standard deviation (std) of the error values are computed. Table 1 shows the results. In Table 1, the error values with the deformed partial scan (i.e. $\mathbf{X}$) are included in the second to fourth columns while those with the deformed full scan are shown in the last three columns. Because of the deformation in $\mathbf{X}$, all methods cannot recover the rigid transformation very accurately. We should notice that the error values shown in Table 1 can be further reduced (if not significantly) by first conducting a coarse registration through incorporating reliably identifiable, salient anatomical features. Two conclusions are drawn by carefully looking into Table 1: (1) HMM(anisotropic) and HMM (isotropic) outperform the rigid CPD method significantly when only partial scan of the whole liver is available intra-operatively, which is the case in laparoscopic surgery [14]; (2) The rigid registration error values with full liver scans are significantly smaller than those with partial scans using all methods.

[1] http://opencas.webarchiv.kit.edu/.

[2] $\theta_{deg} = \arccos\left[\frac{\text{tr}(\mathbf{R}^g\mathbf{R}^{\mathsf{T}})-1}{2}\right]/\pi \times 180$, where $\mathbf{R}^g$ and $\mathbf{R}$ denote the ground-truth and the computed rotation matrix using one specific test method, respectively.

Table 1. The mean and standard deviation of the rotational error values when the three liver models are computed and shown. All the presented results are in the degree unit. The CPD [11] and the HMM (isotropic) methods [7] are compared.

	Liver 1 (Partial)	Liver 2 (Partial)	Liver 3 (Partial)	Liver 1 (Full)	Liver 2 (Full)	Liver 3 (Full)
CPD	38.66 ± 4.65	33.08 ± 2.98	49.17 ± 7.58	9.08 ± 0.65	10.46 ± 0.81	9.22 ± 0.97
HMM	8.40 ± 0.43	$\mathbf{6.18 \pm 0.49}$	14.50 ± 0.86	$\mathbf{8.74 \pm 0.18}$	7.68 ± 0.44	$\mathbf{5.67 \pm 0.31}$
Ours	$\mathbf{8.22 \pm 0.37}$	6.81 ± 0.66	$\mathbf{13.79 \pm 0.92}$	8.79 ± 0.21	$\mathbf{7.39 \pm 0.51}$	6.23 ± 0.38

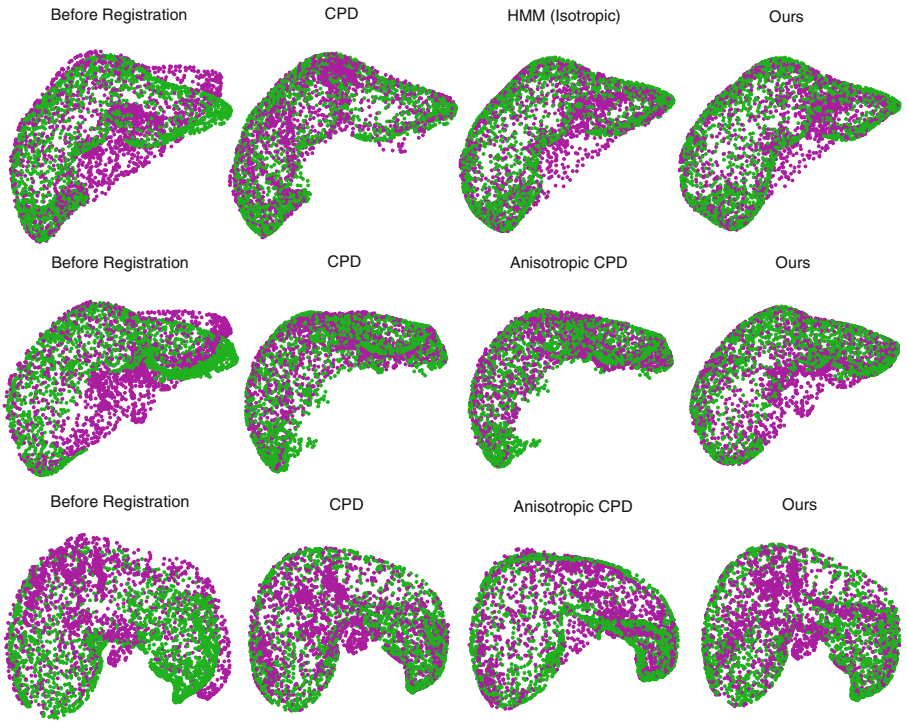

Fig. 1. The registration performances on the three liver models are shown in the three rows respectively. The two point sets before and after registration are shown in the first and in the last three columns respectively. In all sub-figures, the model and data points are represented with red and green dots respectively. The rigid HMM (anisotropic) together with the anisotropic non-rigid CPD is "ours". (Best viewed in color.)

Non-rigid Registration Performance. Since we have noticed in Table 1 that both CPD and HMM (isotropic) cannot well recover the rigid transformation, to have a fair comparison of the non-rigid registration, no gross misalignment between $\mathbf{X}$ ($\mathbf{D}_x$) and $\mathbf{Y}$ ($\mathbf{D}_y$) exists in this section. Besides, all the deformed scans (i.e. $\mathbf{X}$) are partial. To begin with, $\mathbf{X}$ ($\mathbf{D}_x$) and $\mathbf{Y}$ ($\mathbf{D}_y$) are downsampled to $N_{test} = 2000$ points. With all three liver models, the inputs into non-rigid

CPD [11] include the sampled $\mathbf{X}$ and $\mathbf{Y}$. With all three liver models, the inputs into anisotropic CPD (introduced in Sect. 2.2) are the sampled $\mathbf{X}$ and $\mathbf{Y}$. With all three liver models, the sampled $\mathbf{D}_x$ and $\mathbf{D}_y$ are first fed into both HMM (isotropic) [7] or HMM (anisotropic) (i.e denoted as ours), afterwards $\mathbf{X}$ and the rigidly aligned $\mathbf{Y}$ are fed into anisotropic CPD. With Liver 1, we do not show the results using anisotropic CPD since the results with anisotropic CPD are very similar with those using the CPD method. With Liver 2 and Liver 3, we do not show the results with HMM(isotropic) method, since the results with HMM(isotropic) are very similar with those using HMM (anisotropic). The qualitative results are shown in Fig. 1, where the data and model PSs $\mathbf{X}$ and $\mathbf{Y}$ are represented with green and red dots respectively. Comparing the last three subfigures in the first row in Fig. 1, we find that (a) HMM (anisotropic) performs similarly as HMM (isotropic) [7] does, which can be explained by the fact that there exists no noise in $\mathbf{X}$; (b) with CPD all the points in $\mathbf{Y}$ (red) are warped to all the points in $\mathbf{X}$ (green) in the end, which reflects the CPD's vulnerability to partial scan. In the second row, CPD alone or anisotropic CPD alone finds the wrong correspondences. In contrast, with our framework, the points in $\mathbf{X}$ (green) are computed to correspond to the correct corresponding partial region in $\mathbf{Y}$ (red). By carefully observing the figures (especially the edges) in the third row, we can find that ours can best register the two PSs. To briefly conclude, our proposed framework can find the correct correspondences with all three partial liver models and do the registration successfully.

Anisotropic CPD's Robustness to Positional Noise. As we have found in the last section, either only non-rigid CPD or only anisotropic non-rigid CPD without the assistance of normal vectors will fail to find correct correspondences with partial intra-operative data. Thus, to have an effective comparison, CPD only and anisotropic CPD only are compared on the liver data with full intra-operative (or deformed) scan. Different levels of noise vectors are injected into $\mathbf{X}$, and afterwards $\mathbf{X}$ and $\mathbf{Y}$ are normalized to zero mean and unit variance to make the comparisons fair. The noise vectors are sampled from a specific covariance matrix $\mathbf{\Sigma}_{\text{test}} = a \times \text{diag}[0.01, 0.01, 9 \times 0.01]$. Notice that in $\mathbf{\Sigma}_{\text{test}}$ the standard deviation in the z direction is set to be three times of those in x and y directions to mimic the real surgical scenarios (e.g. stereo reconstruction in the laparoscopic liver surgery). The values of $a \in \mathbb{R}$ are set to increase from one to five to test the methods' robustness to noise levels. The mean surface distance (MSD) of registration is defined as the distance between computed $\mathbf{T}(\mathbf{Y})$ using CPD or anisotropic CPD and the ground-truth corresponding points' positions in the ground-truth deformed $\mathbf{Y}$[14]. The above process is repeated for $N_{\text{repeat}} = 1000$ times, and the mean and std of MSD values can be computed. Figure 2 summarizes the corresponding results. As it is shown in Fig. 2, anisotropic CPD achieves smaller MSD values in all test cases than CPD does. In addition, our method is much more robust to the noise levels than the CPD method is with all three liver data sets. All results have passed the statistical tests (paired t-tests with the significance level $\alpha = 0.05$).

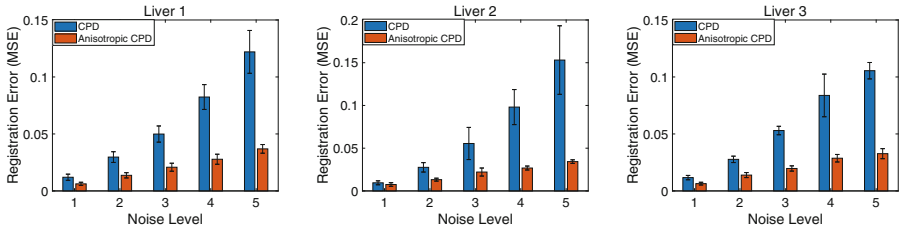

Fig. 2. From left to right, the mean and standard deviation of the registration error values (MSE) are plotted for Liver 1, Liver 2, and Liver 3.

4 Conclusions

We first show that HMM (anisotropic) can recover the rigid transformation matrix than both HMM (isotropic) and CPD more accurately (or at least comparable). This is attributed to the use of more descriptive features (i.e. normal vectors) and the anisotropic positional noise assumption. Another advantage of the proposed method is its great robustness to partial overlapping of pre-operative and intra-operative scans, which is the case in laparoscopic surgery. Finally, we demonstrate that the anisotropic CPD is much more robust to positional noise than CPD due to the generalized anisotropic noise assumption. A limitation of this paper is that we only test our methods on the liver models. In the future, we will apply our algorithm to cardiac surgery and neurosurgery that involve deformation. Another future work is to utilize the joint registration method of multiple point sets [8] in the rigid step of our non-rigid registration framework.

Acknowledgement. This project is partially supported by the Hong Kong RGC GRF grants 14210117, RGC NSFC RGC Joint Research Scheme N_CUHK448/17 and the shenzhen Science and Technology Innovation projects JCYJ20170413161616163 awarded to Max Q.-H. Meng.

References

1. Bayer, S., et al.: Intraoperative brain shift compensation using a hybrid mixture model. In: Frangi, A.F., Schnabel, J.A., Davatzikos, C., Alberola-López, C., Fichtinger, G. (eds.) MICCAI 2018. LNCS, vol. 11073, pp. 116–124. Springer, Cham (2018). https://doi.org/10.1007/978-3-030-00937-3_14
2. Cignoni, P., Callieri, M., Corsini, M., Dellepiane, M., Ganovelli, F., Ranzuglia, G.: MeshLAB: an open-source mesh processing tool. In: Eurographics Italian Chapter Conference, pp. 129–136 (2008)
3. Collins, J.A., et al.: Improving registration robustness for image-guided liver surgery in a novel human-to-phantom data framework. IEEE TMI **36**(7), 1502–1510 (2017)
4. Luo, J., et al.: Using the variogram for vector outlier screening: application to feature-based image registration. IJCARS **13**(12), 1871–1880 (2018)

5. Min, Z., Ren, H., Meng, M.Q.H.: Statistical model of total target registration error in image-guided surgery. IEEE TASE (2019). https://doi.org/10.1109/TASE.2019.2909646
6. Min, Z., Wang, J., Meng, M.Q.-H.: Joint registration of multiple generalized point sets. In: Reuter, M., Wachinger, C., Lombaert, H., Paniagua, B., Lüthi, M., Egger, B. (eds.) ShapeMI 2018. LNCS, vol. 11167, pp. 169–177. Springer, Cham (2018). https://doi.org/10.1007/978-3-030-04747-4_16
7. Min, Z., Wang, J., Meng, M.Q.H.: Robust generalized point cloud registration using hybrid mixture model. In: ICRA 2018, pp. 4812–4818. IEEE (2018)
8. Min, Z., Wang, J., Meng, M.Q.H.: Joint rigid registration of multiple generalized point sets with hybrid mixture models. IEEE TASE (2019). https://doi.org/10.1109/TASE.2019.2906391
9. Min, Z., Wang, J., Meng, M.Q.H.: Robust generalized point cloud registration with orientational data based on expectation maximization. IEEE TASE (2019). https://doi.org/10.1109/TASE.2019.2914306
10. Min, Z., Wang, J., Song, S., Meng, M.Q.H.: Robust generalized point cloud registration with expectation maximization considering anisotropic positional uncertainties. In: IROS 2018, pp. 1290–1297. IEEE (2018)
11. Myronenko, A., Song, X.: Point set registration: coherent point drift. IEEE Trans. Pattern Anal. Mach. Intell. **32**(12), 2262–2275 (2010)
12. Ravikumar, N., Gooya, A., Beltrachini, L., Frangi, A.F., Taylor, Z.A.: Generalised coherent point drift for group-wise multi-dimensional analysis of diffusion brain MRI data. Med. Image Anal. **53**, 47–63 (2019)
13. Ravikumar, N., Gooya, A., Frangi, A.F., Taylor, Z.A.: Generalised coherent point drift for group-wise registration of multi-dimensional point sets. In: Descoteaux, M., Maier-Hein, L., Franz, A., Jannin, P., Collins, D.L., Duchesne, S. (eds.) MICCAI 2017. LNCS, vol. 10433, pp. 309–316. Springer, Cham (2017). https://doi.org/10.1007/978-3-319-66182-7_36
14. Robu, M.R., et al.: Global rigid registration of ct to video in laparoscopic liver surgery. Int. J. Comput. Assist. Radiol. Surg. **13**(6), 947–956 (2018)
15. Sinha, A., Liu, X., Reiter, A., Ishii, M., Hager, G.D., Taylor, R.H.: Endoscopic navigation in the absence of CT imaging. In: Frangi, A.F., Schnabel, J.A., Davatzikos, C., Alberola-López, C., Fichtinger, G. (eds.) MICCAI 2018. LNCS, vol. 11073, pp. 64–71. Springer, Cham (2018). https://doi.org/10.1007/978-3-030-00937-3_8
16. Suwelack, S., et al.: Physics-based shape matching for intraoperative image guidance. Med. Phys. **41**(11), 111901 (2014)